Chapter 3. Optics

A.Drozhdin, A.Garren, N.Gelfand, C.Johnstone,
L.Michelotti, S.Ohnuma, G.Rees, D.Ritson

The lattice chosen for PD2 differs from that of PD1 in several respects: saliently, (a) it is a superperiod 2 racetrack, instead of a superperiod 3 triangle, (b) it has 2/3 the circumference, and (c) its kinetic energy range is less than half. In this chapter we describe its optics. Conclusions drawn from this material must be tempered with the understanding that "optics" refers to the behavior of one and only one proton traversing a fixed, static electromagnetic environment. It especially refers to those features of particle orbits that scale with the ratio of magnetic field to momentum. Consideration of other phenomena, such as space charge and impedance effects, is relegated to other chapters.

The structure of this chapter is similar to that of its counterpart in the PD1 Report [1], which is assumed as background. Some information that can be found there is not repeated here. The first section contains a list of constraints under which lattice designs and ideas were considered. Descriptions of the arcs and straight sections of the PD2 lattice is provided in Section 3.2. Further examination of its optical properties, including discussions of resonance excitation and errors, is postponed to Section 3.3.

Several possible designs were considered before settling upon one, but the decisions that were made may not be final. They are, nonetheless, the ones under which this study was conducted. A few promising alternatives will be presented in Section 3.4.

3.1. Requirements, Constraints, and Features

Design of the PD2 lattice was constrained and influenced by a number of criteria, ranging from requirements to desiderata. These included:

Length The Proton Driver's circumference was set to 474.2 m, to match that of Fermilab's Booster. This constraint severely limits the amount of space available for utility hardware. If considered desirable or necessary, it could be enlarged in a later revision, either (a) by adding cells to the straight sections or (b) by increasing the length of its standard cell (see below). In the latter case, focusing must also increase to maintain the Driver's optical properties.

Energy range For PD2, injection energy of the Proton Driver was raised from 400 MeV to 600 MeV, and extraction energy lowered from 16 GeV to 8 GeV, for transfer into the Main Injector. At the Driver's length of 474.2 m, the protons' revolution frequency will thus vary from 501 kHz (2.00 μsec) to 629 kHz (1.59 μsec).

Transition We avoid transition effects in the Proton Driver by requiring γ_t to be beyond the reach of the extraction energy. Thus, it is required that $\gamma_t > 9.5$, or, equivalently, that the momentum compaction $\alpha = 1/\gamma_t^2 < 0.011$.

Momentum acceptance The large momentum acceptance of $\pm$ 2.5 % used in PD1 was predicated on using the Driver as front end to a neutrino factory or muon collider. In this study, the required acceptance has been reduced to $\pm$ 1 %, suitable for transfer to the Main Injector.

Transverse acceptance Tune spread within the beam due to space charge can be as large as 0.25. In order to make this as small as possible, painting will be used to flatten the transverse charge distribution. We require that transverse beam emittance, after painting and including space charge effects, be no larger than 40 π mm-mr (normalized, 95%). The Proton Driver must accept 40π mm-mr invariant emittance in both planes. To achieve this, emphasis was placed on minimizing the maximum values of lattice functions, β_x and β_y, and horizontal dispersion, D. In the course of the study, a criterion was informally established that set upper bounds of $\beta \leq 20\,\mathrm{m}$ and $D \leq 2.5\,\mathrm{m}$. Together, these assure a maximum horizontal excursion of $\approx \pm 5\,\mathrm{cm}$ from the closed orbit, evenly divided between dispersion and emittance.

Phase advance Although it has not been observed in proton machines, it is prudent to avoid any possibility of synchro-betatron coupling resonances [2], especially in view of a relatively large value of synchrotron frequency, ($\nu_s \approx 0.06$), at low energies. This is done by zeroing the chromaticity with sextupoles in the arcs and the dispersion in the straight sections, where RF cavities will be placed. To assure this, the horizontal phase advance through an arc was required to be a multiple of 2π.

Dynamic aperture The dynamic aperture of the Proton Driver, calculated with chromaticity sextupoles powered but no other significant sources of nonlinearity, is required to exceed $3 \times 40\pi$ mm-mr (invariant, transverse) emittance for the entire momentum spread range of $\pm 1\%$.

Straight sections Two long straight sections will be used for injection, extraction, and acceleration. Collimation will be done in the arcs. Considerations given to the design of the two long straight sections included:

Superperiodicity Trim quads in the straight sections will be used to tune the Proton Driver to a good working point. It is highly recommended that they be powered symmetrically across the Driver so as to maintain its superperiodicity.

Injection The beam's size at the stripping foil should be large enough to prevent excessive temperatures. At the same time, large β functions at the foil contribute to emittance growth, due to multiple Coulomb scattering. The compromise choice of $\beta_x \approx \beta_y \approx 10\,\mathrm{m}$ satisfies these requirements. In the doublet lattice of the straight section the foil can be located between the focusing and defocusing quadrupoles of a doublet. This permits the use of a defocusing quadrupole for injection and circulating beams separation, upstream of the foil, at the injection Lambertson magnet, and it permits the use of a focusing quadrupole for

separation of the H^0 component and of circulating beam behind the foil at the entrance to the neutral beam dumper. Drift spaces between the adjacent doublets upstream and downstream must be large enough to accommodate both H^- injection and dumping of the H^0 component. The phase advance between the first and last kicker magnets for painting, located on each side of the foil, should be close to 180° so that the required kicker strength is not excessive.

Extraction The phase advance between kickers and septa as well as lattice functions at various extraction devices should be chosen carefully in order not to make excessive demands on magnets. The system should be able to accommodate at least twice the 95% beam emittance, $\varepsilon_{inv} = 40\pi$ mm-mr, so that no halo scraping occurs in any extraction magnet.

RF It is intended to reuse RF cavities from the current Fermilab Booster in the Proton Driver's straight sections. The cavities are 2.35 m long, and at least 21 will be needed, requiring 49.35 m of empty space. If there is at least 7.05 m between quadrupoles, three of these cavities can be placed within a straight section cell.

Collimation Large β functions and dispersion are necessary at the primary collimators. The phase advance over the collimation system should not be less than 180° in both directions.

Magnets We will write criteria for magnetic field errors in Section 3.3.4. Here, we touch upon three properties.

Peak fields In order that quadrupoles and dipoles track well during the ramp, while avoiding both saturation and excessive power loss, it was decided early to limit the maximum field in dipoles to 1.5 T and the peak gradient of quadrupoles to 10 T/m. Further, a maximum kick angle of 5 mrad is imposed for dipole correctors.

Spacing Because of fabrication requirements for magnet ends and bellows, minimal spacings between quadrupoles and dipoles were established: the minimum space between the quadrupoles of a doublet was set to 47 cm; the minimum space between a quadrupole and a dipole, to 85 cm.

Edge focusing To mitigate the sagitta problem, dipoles will be bent into an arc corresponding to the radius of curvature of the closed orbit. However, the faces of a dipole will remain parallel. The impact of vertical edge focusing on lattice functions and tune must be taken into account in designing the Proton Driver.

3.2. Lattice Description

Based primarily on considerations of available space and the size of lattice functions, a racetrack configuration was chosen for PD2: two 75.44 m straight sections connected by two 161.66 m, 180° arc sections, making its circumference of 474.20 m identical to the current Fermilab Booster's, as required. The racetrack structure leads to longer straight

sections and ability to design arcs that give higher transition energy. In this section we'll describe the pieces of this lattice.

3.2.1. Overview

The Proton Driver is partitioned into forty-four 10.777 m cells, 15 for an arc and 7 in a straight section. Each cell contains a defocusing (D) and focusing (F) quadrupole doublet on the main bus and a corresponding pair of independently powered trim quads. Their peak gradients, at 8 GeV extraction (kinetic) energy, are $\pm$ 10 T/m. The F quad is 1.262 m long, the D quad, 1.126 m, and they are separated by 47 cm. Trim quads, positioned just outside the doublet, are 20 cm long; each is separated by 19 cm from its counterpart.

This leaves about 7.1 m of empty space in each cell. In the arcs, they will be filled with dipoles and collimation hardware; in the straight sections, with hardware for injection, extraction, and acceleration. Additional diagnostic and control devices – beam position monitors, orbit correctors, dampers, and the like – must fit into whatever space remains.

3.2.2. Arc module

Each arc is organized into 5 modules of 3 cells, 15 cells in all. Quadrupole lengths were chosen so as to produce a phase advance per module of $(\Delta\psi_x, \Delta\psi_y)|_{\text{module}} = (8\pi/5, 6\pi/5)$ which sets the average phase advance per cell to be $(\Delta\psi_x, \Delta\psi_y)|_{\text{cell}} = (8\pi/15, 2\pi/5)$ $= (96^\circ, 72^\circ)$. A horizontal phase advance close to 90° is convenient for injection and extraction. Because the total phase advance across an arc is $(\Delta\psi_x, \Delta\psi_y)|_{\text{arc}} = (8\pi, 6\pi)$, it is, to first order, optically transparent: its 4×4 transfer matrix is the identity. Thus, the arcs will preserve lattice functions, including zero dispersion, across the straights. If the phase advance per cell were exactly repeated throughout the racetrack, the Proton Driver's tunes would be $(\nu_x, \nu_y) = (11.73, 8.80)$.

The two outer cells of an arc module contain a large dipole (5.646 m, 16.2° bend) and the inner cell a small one (1.188 m, 3.4° bend). Their lengths were chosen so as to create a first order achromatic bend, thus zeroing the dispersion between modules. As a stand-alone periodic unit, the lattice functions of a single arc module would be as shown in Figure 3.2.1.

Four chromaticity correcting sextupoles are placed in each arc module. To conserve space, they replace the four trim quadrupoles closest to the short dipole. Alternatively, it may be possible, and perhaps preferable, to build a correction package consisting of quadrupole and sextupole. If not, then we must rely on two trim quads to control the phase advance through each module.

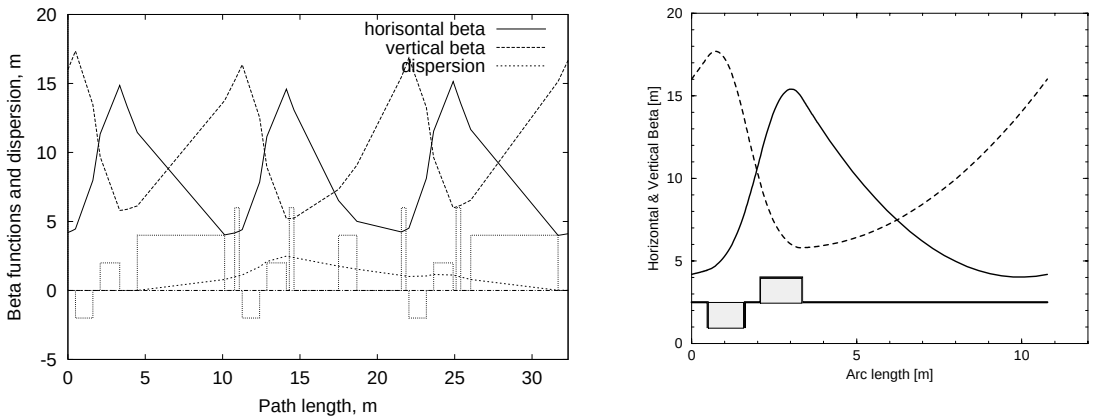

Figure 3.2.1. Lattice functions of (a) an arc module and (b) a straight section's cell, treating each as a periodic unit.

3.2.3. Straight section

The seven cells in each straight section do not contain dipoles, and the absence of edge focusing distorts the lattice functions (esp., β_y) slightly. Lattice functions for a single straight section cell, treated as a periodic unit, are shown in Figure 3.2.1.; its phase advance is $(\Delta\psi_x, \Delta\psi_y)|_{\text{cell}} = (8\pi/15, 0.96 \cdot (2\pi/5))$. In fact, these *are* its lattice functions in the base configuration, because of the arcs' optical transparency.

3.2.4. Hardware and space allocations

The use of similar cells in the arcs and long straight sections, identical except for the presence of dipoles in the arcs, allows for just four kinds of magnets powered on the main bus: 2 quadrupoles, and 2 dipoles. The F and D quadrupole strengths are equal and opposite; the two dipoles likewise have equal fields, but all four have different lengths. It is possible to obtain a reasonable beta function match between the arcs and straight sections while minimizing the number of magnets with different lengths.

The magnetic hardware and their space usage in the PD2 lattice are tabulated below. Only magnetic lengths are included in this table; they do not include the physical ends of elements. Using these numbers, dipoles take up 26.32% of the lattice, main bus quads, 22.16%, chromaticity correcting sextupoles, 2.53%, and trim quadrupoles, 2.02%.

3.2.5. Nomenclature

In order to identify the components in the Proton Driver a system of nomenclature has been devised so that the location, and to some extent the function, of an element can be inferred

Lattice	Element	Name	Number	Length [m]		Field	
PD2	DIPOLES	B1	2x5x2 = 20	5.646	B =	1.49	T
		B2	5x2 = 10	1.188		1.49	
	QUADRUPOLES	QF	(3x5+7)x2 = 44	1.262	B' =	10.02	T/m
		QD	(3x5+7)x2 = 44	1.126		-10.02	
		QDT<N>	(5+7)x2 = 24	0.200	B' =	0.00	T/m
		QFT<N>	(5+7)x2 = 24	0.200		0.00	
	SEXTUPOLES	SF	2x5x2 = 20	0.300	B''=	49.10	T/m^2
		SD	2x5x2 = 20	0.300		-71.05	
	FREE (total)			222.728			

Table 3.2.1. Hardware and space usage in the PD2 lattice.

from its name. The direction of the beam is clockwise and our naming system will follow the direction of the beam. It will be easier to follow the description below by referring to the graphical layout of the Proton Driver contained in Chapter 2.

The system involves dividing the ring into four logical groupings, or sectors, of the elements. The first sector is an arc, denoted as P10, consisting of five modules of three cells. Each cell contains a quadrupole doublet and a bending magnet. The quadrupoles will be assigned a name that reflects (a) their horizontal focusing properties, QD or QF, (b) the sector, (c) the module, and (d) the cell. Thus, QDijk will mean a horizontally defocusing quadrupole in the kth cell of the jth module in the ith sector: the first quadrupoles in the first sector will be named QD111 and QF111, and the last quadrupoles in this sector will be QD153 and QF153.

The arc, P10, is followed by a straight section, P20, consisting of 7 cells, each with a quadrupole doublet. To resolve the superperiod 2 ambiguity, we identify P20 as the sector containing injection hardware, in addition to RF cavities. The quadrupoles will be assigned a name that reflects (a) their horizontal focusing properties, QD or QF, (b) the sector number, (c) 0 for the module number, (d) and the cell number. QD$i0k$ will mean a horizontally defocusing quadrupole in the kth cell in the ith sector. Thus, the first quadrupoles in the second sector will be named QD201 and QF201. The last quadrupoles in this sector will be QD207 and QF207.

The injection straight P20 is followed by the arc sector P30 where collimation takes place. As in the arc P10 there are 5 modules each consisting of 3 cells. The naming convention is the same as in P10 except that the magnet names have the value of 3 for the sector number. The ring is completed with another straight section P40 that contain RF and extraction elements. Its naming scheme is similar to that of section P20.

3.3. Analysis

The complete lattice functions for half of the racetrack, with one arc joined to one straight section, are shown in Figure 3.3.2. The vertical beta wave is caused by edge focusing in the dipoles, or, alternatively, its absence in the straight section cells. The arcs' optical trans-

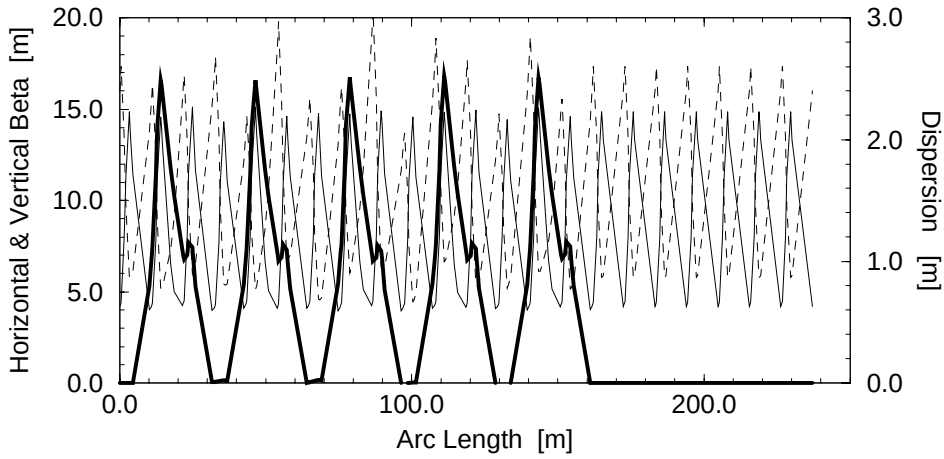

Figure 3.3.2. Lattice functions for half the racetrack: β_x is plotted as a solid line, β_y as a dashed line, and D as a dark solid line.

parency confines the wave; it does not propagate into the straight sections. The actual tunes associated with the base configuration are shifted from $(11.73, 8.80)$ to $(11.747, 8.684)$. That point is shown as a dark circle in Figure 3.3.3., wherein are drawn the sum resonance lines up to fourth order.

As an exercise, families of trim quadrupoles in the straight section were used to move the tunes to $(11.880, 8.850)$, the point shown as an open circle in Figure 3.3.3., without breaking superperiodicity. In the sections to follow, we will refer to this as the "tuned configuration." Lattice functions are, of course, perturbed slightly in the process. Tuning was done in such a way that the vertical beta wave was transferred from the arcs to the straight sections.

The tunes identified in Figure 3.3.3. refer to single particle optics. In reality, space charge will reduce the tunes of particles in the core of the beam by an amount that will depend on painting. (See Chapter 4.) Protons undergoing large amplitude oscillations will be less affected by space charge, but their tunes will increase (slightly) due to the presence of chromaticity correcting sextupoles, as will be discussed on page 3 - 9. The combined effects of space charge and sextupole fields (and octupole error fields) will spread the tunes away from the displayed points in opposite directions. The single particle "optical tune," the "working point," acts as a reference for this distribution. Maximum spread will occur at injection. As the beam's energy increases, the distribution will collapse into the working point. Space charge forces will decrease, as $v/c \to 1$, shrinking the distribution

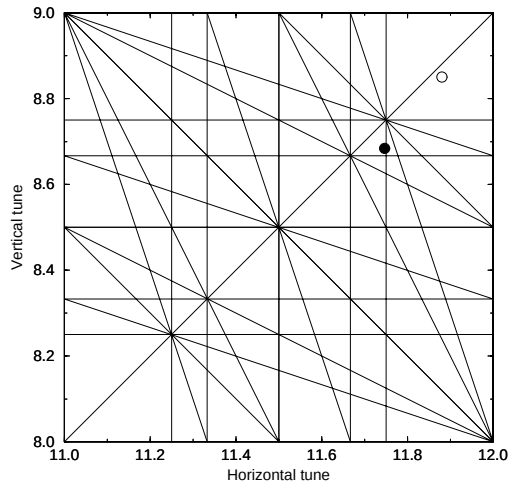

Figure 3.3.3. Tune diagram. The Proton Driver's base lattice (dark circle) has tunes (11.747,8.684). A possible tuned lattice (white circle) is shown with tunes (11.880,8.850).

from below, and the sextupole/octupole tune spread will decrease, as emittances become smaller, shrinking the distribution from above.

3.3.1. Chromatic properties

The natural chromaticities of the PD2 base configuration – normalized as $\Delta\nu = \xi \Delta p/p$ – are $(\xi_x, \xi_y) = (-13.61, -11.88)$. These are zeroed by powering the sextupoles placed in the arc modules to $B'' = 49$ T/m^2, near the F quad, and $B'' = -71$ T/m^2, near the D quad. (In the tuned configuration these values are only slightly different: $B'' = 50$ T/m^2 and $B'' = -73$ T/m^2.) Chromaticity in the actual Proton Driver undoubtedly will not be set to zero but to some small negative value, since the machine will run below transition. Thus, the actual values of B'' will be marginally smaller, mitigating somewhat the magnitude of effects discussed in the rest of this report.

Because each module is a first order achromat, dispersion is small in the vicinity of its two outer dipoles. The contribution from the shorter, central dipoles to the momentum compaction can be estimated by assuming a horizontal dispersion of 1.7 m at that location.

$$\langle D/\rho \rangle \approx \frac{1.7\,\mathrm{m}}{29.7\,\mathrm{Tm}/1.49\,\mathrm{T}} \cdot \frac{1.19\,\mathrm{m} \cdot (5 \cdot 2)}{474.2\,\mathrm{m}} = 0.0021$$

This accounts for 40% of the total momentum compaction, which is $\alpha = 0.00528$, making $\gamma_t = 13.8$, comfortably larger than 9.5.

The chromaticities, ξ_x, ξ_y, considered not as constants but as functions of $\Delta p/p$, are plotted in Figure 3.3.4. for the extended range $|\Delta p/p| \leq 0.02$. ξ_y is nearly flat for negative

$\Delta p/p$, with a variation of less than 0.5 over the entire range. On the other hand, ξ_x increases monotonically, only slightly faster than linearly, by more than 2.5. The overall variation across $\pm$ 1% is small.

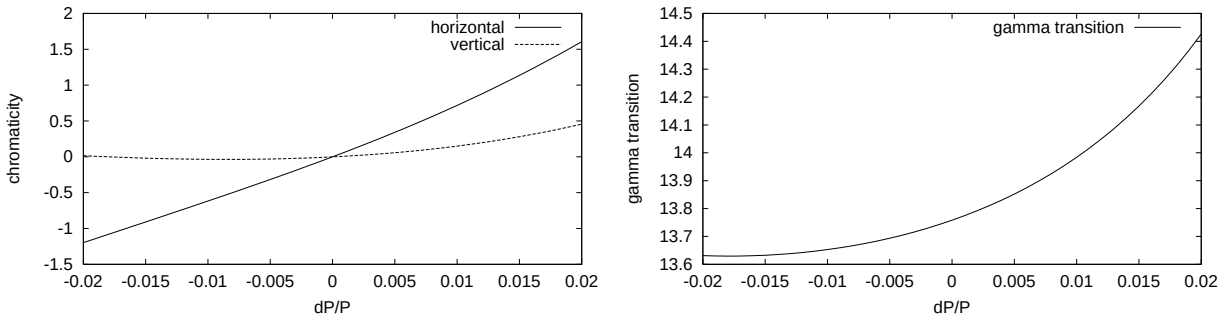

Figure 3.3.4. Proton Driver chromaticity and γ_t.

The corresponding plot of γ_t vs. $\Delta p/p$ is the almost exponential looking curve displayed on the right in Figure 3.3.4. Its variation is of little concern, because all of these values are larger than required.

Lattice functions, β_x, β_y, and D, take on perturbed values when $\Delta p/p \neq 0$. Their maxima are plotted, as functions of $\Delta p/p$, in Figure 3.3.5. The variations of $\beta_{y,\max}$ and $D_{\max}$ are

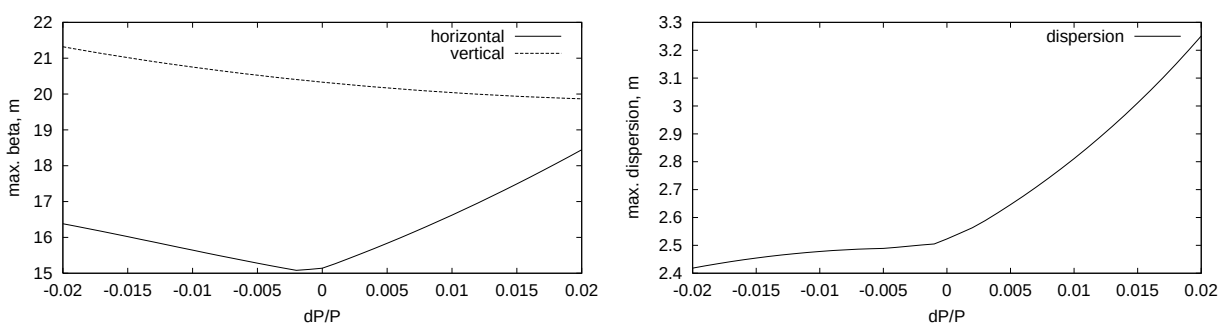

Figure 3.3.5. Proton Driver maximum β functions and dispersion.

monotonic, while $\beta_{x,\max}$ goes through a minimum near $\Delta p/p = 0$. As in the previous figures, there is larger variation for positive than negative $\Delta p/p$. Estimates of the closed orbit based on the value $D|_{\Delta p/p=0}$ should be increased by $\approx$ 12% at the momentum acceptance limit, $\Delta p/p = 1\%$.

3.3.2. Tune footprint

The sextupoles used to zero chromaticity will produce an amplitude dependent tune shift proportional to the square of their excitation. Second order perturbation theory predicts,

for the PD2 base configuration,

$$\begin{aligned}\Delta\nu_x &= 0.120\,\varepsilon_x/\pi + 0.114\,\varepsilon_y/\pi \\ \Delta\nu_y &= 0.114\,\varepsilon_x/\pi + 0.230\,\varepsilon_y/\pi \ ,\end{aligned}$$

where $\Delta\nu$ is given in units of 10^{-3} and ε is in mm-mr.[1] For the tuned configuration, the coefficients are somewhat larger.

$$\begin{aligned}\Delta\nu_x &= 0.126\,\varepsilon_x/\pi + 0.397\,\varepsilon_y/\pi \\ \Delta\nu_y &= 0.397\,\varepsilon_x/\pi + 0.384\,\varepsilon_y/\pi\end{aligned}$$

The upper limit on transverse emittance is $\varepsilon_{\rm inv} \leq 40\pi$ mm-mr, so that

$$\begin{aligned}\varepsilon/\pi = \frac{\varepsilon_{\rm inv}/\pi}{\beta\gamma} &\leq \frac{40}{9.47} = 4.22 \ \ \text{mm-mr} \quad \text{at extraction} \\ &\leq \frac{40}{1.30} = 30.8 \ \ \text{mm-mr} \quad \text{at injection.}\end{aligned} \tag{3.1}$$

Even at injection into the tuned configuration, the vertical tune spread resulting from sextupole excitation will only be about 0.02.

3.3.3. Dynamic aperture

The dynamic aperture of the PD2 lattice has been estimated by tracking. Only the dipoles, quadrupoles, and chromaticity sextupoles have been included. Again, this is single particle tracking within a static magnetic environment: it does not include space charge, synchrotron oscillations (with or without non-zero chromaticities), or magnet ramping; also not included are systematic or random error fields. The results obtained should be considered an upper bound on the actual dynamic aperture. Fortunately, it turns out to be a large upper bound. Its actual (theoretical) value will have to be determined by more detailed studies, especially including space charge and RF.

Since "dynamic aperture" is an ambiguous concept, we will first describe the procedure that was used. A particle was launched from a point $(x,y), x,y \gg 0$, with $x' = y' = 0.0$. If the particle failed to complete 10^5 turns, the value of y was reduced and the tracking started again. When the particle survived for 10^5 turns the initial point, $(x, y_{\rm max})$, was considered inside the dynamic aperture. Once a stable orbit was found, x was decreased, y was reset to a large value, and the entire process was repeated, down to $x = 0$. The set of pairs $\{(x, y_{\rm max})\}$ were then converted into normalized emittances using the values of the lattice functions at the initial point.

The results, at the injection energy of 600 MeV, where dynamic aperture is smallest, are shown in Figure 3.3.6. Along the diagonal, the dynamic aperture is at $\varepsilon_{\rm inv} \approx 10 \times 40\pi$ mm-

[1] This is written using "emittance" notation, ε, but, since we are dealing with a single particle, ε is more properly interpreted as an action (or amplitude) coordinate, I, according to $\varepsilon/\pi = 2I$.

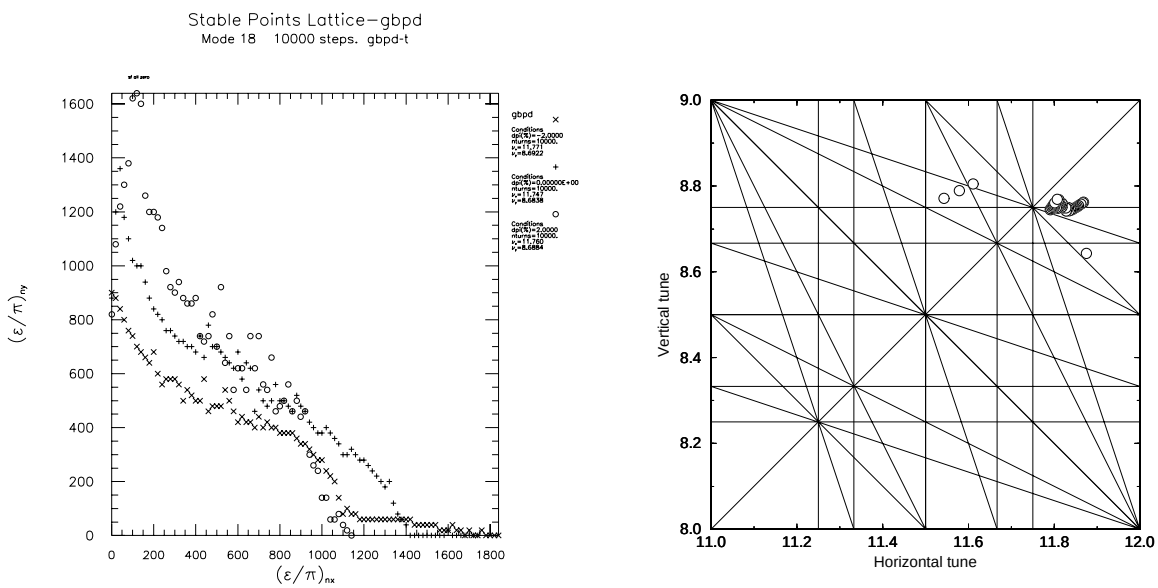

Figure 3.3.6. Dynamic aperture: (a) Scatter plot of largest amplitude stable orbits at $\Delta p/p = 0$ and $\pm 2\%$. (b) Tunes of orbits at the boundary of the dynamic aperture.

mr. For purely horizontal orbits it increases to $\varepsilon_{\rm inv} \approx 25 \times 40\pi$ mm-mr, and for mostly vertical orbits[2] it is slightly less, $\varepsilon_{\rm inv} \approx 20 \times 40\pi$ mm-mr. The interior of this region was scanned further to make certain that the stable orbits defining the dynamic aperture were not caused fortuitously by isolated stable regions (islands) in an otherwise unstable portion of phase space.

Peaks of the tune spectra were calculated for all orbits just inside the dynamic aperture. The right hand side of Figure 3.3.6. shows a scatterplot of these values superposed on the tune diagram of Figure 3.3.3. Clearly, there is a clustering about the line $4\nu_y = 35$, which is excited at second order in the strength of sextupoles. The chromaticity sextupoles both excite this resonance and provide the necessary tune spread to put it within the reach of very large amplitude orbits, as will be discussed in Section 3.3.4.

3.3.4. Errors

We will assume the same estimates for positioning errors that were made in the PD1 Report [1, p.3-12]:

1) transverse quadrupole misalignments: $\sigma_X = \sigma_Y = 0.2$ mm.
2) dipole roll: $\sigma_\Theta = 0.2$ mrad; this will be relaxed to 0.5 mrad.
3) integrated dipole field uniformity: $|\Delta B/B| < 2 \times 10^{-4}$; this will be relaxed to 5×10^{-4}.

[2] Because of the sextupoles, pure vertical orbits are impossible.

These estimates were based on criteria set for alignment of the Antiproton Accumulator. Those which are to be "relaxed" were considered too difficult to achieve reliably.

With regard to field quality, a "flatness criterion" was established in PD1,

$$\text{flatness at } x = x_0 \;\equiv\; \left| \frac{\int dz\, B_y(x = x_o, y = 0, z)}{\int dz\, B_y(x = 0, y = 0, z)} - 1 \right| \quad \text{for dipoles.}$$

For quadrupoles, replace B_y with $B' = G = \partial B_y/\partial x$ in the integrals. Upper bounds for flatness were specified in the PD1 Report [1, p.3-14] at an offset of $x_o = 4$ inches. We adjust them here to an offset of $x_o = 3$ inches: 3×10^{-4} for dipoles and 3×10^{-3} for quadrupoles. In terms of isolated multipoles, this is equivalent to:

dipoles:	$\lvert B^{(2)}/B \rvert$	< 0.1	m^{-2}	$= 0.3$	units
	$\lvert B^{(4)}/B \rvert$	< 214	m^{-4}	$= 0.04$	units
quadrupoles:	$\lvert G^{(2)}/G \rvert$	< 1	m^{-2}	$= 3$	units
	$\lvert G^{(3)}/G \rvert$	< 41	m^{-3}	$= 1$	units

where "unit" refers to the Fermilab convention of "$\times 10^{-4}\,\mathrm{inches}^{-n}$." For now, we continue to accept these as achievable estimates of field quality.

The use of multipoles is complicated by the fact that dipoles are to be bent into an arc. In a straight magnet, the vector potential of the error field – the quantity appearing in Hamiltonian resonance calculations – is expanded in the midplane as,

$$A_3/B = \frac{1}{2} b_1 x^2 + \frac{1}{3} b_2 x^3 + \cdots \quad .$$

When the magnet is bent, curvature terms are added to these coefficients. [3, p.177]

$$A_\phi/B = \frac{1}{2}(b_1 - 1/\rho)x^2 + (b_2/3 - b_1/6\rho + 1/2\rho^2)x^3 + \cdots$$

For the Proton Driver, $1/\rho = 1.5\,\mathrm{T}/29.7\,\mathrm{Tm} = 13 \times 10^{-4}\,\mathrm{in}^{-1}$, or 13 "units." Its interference with b_1 is already accounted for by linear theory. Using the specifications given above, $b_2/3$ will be ≈ 0.1 units, while the curvature terms contribute 0.009 units to the x^3 coefficient. Unless dipoles are constructed extraordinarily well, their error fields will dominate over curvature effects.

3.3.4.1. Closed orbit

To first order, the closed orbit error at point i caused by a kick error, $\Delta x'$, at point j is given by the matrix element [4, p.92],

$$\partial x_i/\partial \Delta x'_j \equiv M_{ij} = \frac{1}{2\sin \pi\nu} \sqrt{\beta_i \beta_j} \cos(\,\psi_i - \psi_j - \pi\nu\,) \quad ,$$

where we assume $0 \le \psi_i - \psi_j < 2\pi\nu$. If the errors are random and uncorrelated,

$$\sigma^2(x_i) = \sum_j M_{ij}^2 \sigma^2(\Delta x'_j)$$

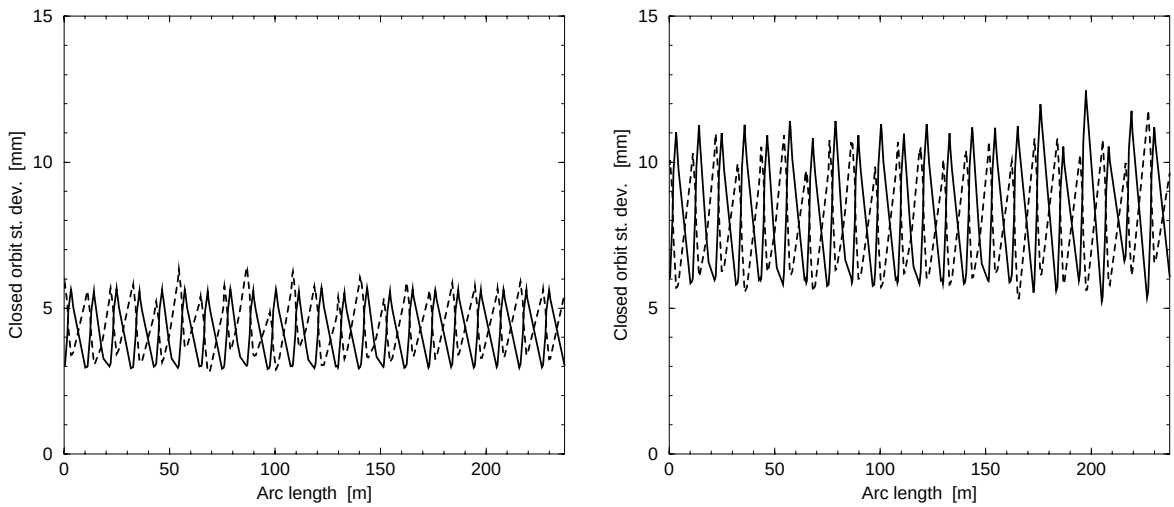

Figure 3.3.7. Closed orbit error standard deviation: base (left) and tuned (right) lattices. Only half the racetrack is shown.

(Ab)using the misalignment errors listed in Section 3.3.4., we can estimate the relevant standard deviations as follows.

$$\begin{aligned}
\text{(a) quad misalignment}: \quad \sigma_{\Delta x'} &= \frac{B'l}{B\rho}\sigma_X \\
\text{(b) dipole roll (small)}: \quad \sigma_{\Delta x'} &= \frac{Bl}{B\rho}\sigma_\Theta \\
\text{(c) field uniformity}: \quad \sigma_{\Delta x'} &= \frac{Bl}{B\rho}\sigma_{\Delta B/B}
\end{aligned}$$

The horizontal closed orbit is affected by (a) and (c); the vertical, by (a) and (b). Results of inserting these into Eq.(3.3.4.) and performing the calculation on the base configuration are shown on the left in Figure 3.3.7. The results for the tuned configuration are shown on the right. In both cases, only half of the racetrack is shown. The larger excursion in the tuned configuration arises (a) mostly from the $\sin\pi\nu$ in the denominator of Eq.(3.3.4.), (b) from slightly larger lattice functions, and (c) from the fact that the trim quads are contributing. The numbers are in reasonable agreement with our crude estimates. The difference in tunes accounts for most of the increase in going from the base lattice to the tuned lattice.

Steering magnets A system of correction dipoles will be necessary to reduce the expected 5-10 mm (or more) excursion of the closed orbit. The specification common to horizontal and vertical directions is that the maximum kick angle of each steering element should be 5 mr. The maximum horizontal and vertical deflections generated by this kick will be 50 mm and 77 mm, respectively. For horizontal kicks, there will be special windings in each dipole. The required kick angle is 1.8% of the bend angle of regular dipoles and 8.4% of short dipoles. Horizontal orbit correction is then possible up to the highest energy.

Vertically, the kick will be provided by 20 cm long steering magnets. A 5 mr vertical kick would require a field of 0.10 T at injection and 0.74 T at extraction. Imposing an upper bound on corrector strength would reduce the maximum (kinetic) energy at which such a kick could be done: e.g., 5.1 GeV for $B_{\rm max} = 0.5\ T$, 2.8 GeV for $B_{\rm max} = 0.3\ T$. Correcting an improbably bad vertical closed orbit beyond this energy would then require realigning quadrupoles. In such a case, it should be possible to select the optimum combination of a specified number of quadrupoles based on BPM readings of the established closed orbit.

There will be no room for correctors in the cells containing RF. Care must be taken to minimize the closed orbit deviation and its derivative at the boundaries of those regions.

3.3.4.2. Tunes

We consider here three isues regarding the Proton Driver's tunes: their adjustment away from the base configuration, linear horizontal-vertical coupling, and the tune footprint caused by chromaticity sextupoles.

Tune adjustment Arc quadrupoles will be responsible for maintaining the phase advance per module in arcs, while quadrupoles in long straights will be used to locate the working point at the optimum position in the tune diagram. It is impossible to predict what this will be. Experience gained in Accumulator and Main Injector operation indicates that, if magnets are constructed carefully, it is not necessary to have the flexibility to explore a wide range of tune values: something less than $\pm$ 0.3 may be sufficient. For the Proton Driver, tune adjustment will be needed for picking a good working point, maintaining the phase advance per module in the arcs, compensating for space charge detuning, and minimizing beam loss during extraction.

We make a representative estimate (at 8 GeV) of the tune correction obtained by powering one trim quad at 1 T/m. Ignoring the orthogonal plane, this is

$$(\Delta\nu_x, \Delta\nu_y) = \frac{1}{4\pi}\frac{B'l}{B\rho}\cdot(\beta_x, \beta_y) = \frac{1}{4\pi}\cdot\frac{1\,\mathrm{T/m}\cdot 0.2\,\mathrm{m}}{29.7\,\mathrm{Tm}}\cdot(14\,\mathrm{m}, 16\,\mathrm{m}) = (0.0075, 0.0086)$$

There are 24 trim quads of each type, but only the 14 in the straight sections would be used for tune control. This provides a tune reach of $(\pm 0.053, \pm 0.060)$ per T/m of excitation.

Tune adjustment can also be done by special windings in each quadrupole. If the gradient in a main bus (QD or QF) quadrupole is adjusted by 1%, the in-plane tune shift would be $\Delta\nu = 0.005$. The 14 main quads in the straight sections would then supply an additional tune reach of $\approx \pm 0.07$ (per 1% variation). Again, these estimates are made ignoring the influence of the orthogonal plane. Taking it into account would extend the reach.

Horizontal-vertical coupling Linear coupling is produced by skew quadrupole components, which can arise from field errors and from rolling normal quads. Its effects will be most pronounced when tunes are near the resonance condition, $\nu_x - \nu_y = n$, where, for the Proton Driver, $n = 3$. Near such resonance, the Hamiltonian is characterized by a dimen-

sionless coupling,

$$g = \frac{1}{2\pi}\left|\sum \frac{B'_{\rm skew} l}{B\rho}\sqrt{\beta_x\beta_y}e^{i(\psi_x-\psi_y-\delta\cdot\Theta)}\right| \ ,$$

where $B'_{\rm skew} = \partial B_x/\partial x$ is the skew coefficient, and $\delta = \nu_x - \nu_y - 3$. If a normal quad is rolled through a small angle, Θ, then $B'_{\rm skew} = B'\cdot 2\Theta$. Following usual procedures, as was done in PD1, we will estimate this term by summing in quadrature, and use σ_Θ for Θ, with the result,

$$\begin{aligned}
\sigma_g &= \frac{1}{2\pi}\cdot 2\sigma_\Theta\left(\sum\left(\frac{B'l}{B\rho}\right)^2\cdot\beta_x\beta_y\right)^{1/2} \\
&\approx \frac{1}{\pi}\cdot 5\times 10^{-4}\cdot\left(44\cdot\left(\frac{10\,\mathrm{T/m}\cdot 1.26\,\mathrm{m}}{29.7\,\mathrm{Tm}}\right)^2\cdot 13\,\mathrm{m}\cdot 7.5\,\mathrm{m}\right. \\
&\qquad\qquad \left. +44\cdot\left(\frac{10\,\mathrm{T/m}\cdot 1.13\,\mathrm{m}}{29.7\,\mathrm{Tm}}\right)^2\cdot 6.0\,\mathrm{m}\cdot 15.3\,\mathrm{m}\right)^{1/2} \\
&= 5.9\times 10^{-3} \ .
\end{aligned}$$

The coupling into transverse amplitudes is $(1+(\delta/g)^2)^{-1/2} \approx (1+(\delta/\sigma_g)^2)^{-1/2}$. For the base configuration, (11.747,8.684), this is about 9%. That is, if the horizontal excursion of the beam is 1 cm, the estimated (r.m.s.) excursion in the vertical direction generated by coupling will be 0.9 mm. This is large enough to consider introducing a few skew quad correctors, to reduce the value of g, or tuning farther from the diagonal, to increase the value of δ.

Sextupole errors in dipoles The contribution of a local sextupolar field to chromaticity is approximated as

$$(\Delta\xi_x, \Delta\xi_y) = \frac{1}{4\pi}\cdot\left(\frac{B''l}{B\rho}\right)\cdot D\cdot(\beta_x, -\beta_y) \ .$$

If $\langle|B''/B_o|\rangle < 0.1\mathrm{m}^{-2}$ in the dipoles, then their contributions to the chromaticity will be

$$\begin{aligned}
(|\Delta\xi_x|, |\Delta\xi_y|) &\approx 20\times(0.006, 0.009), \ \text{for long dipoles,} \\
&\approx 10\times(0.02, 0.03), \ \text{for short dipoles.}
\end{aligned}$$

These values are negligible compared with the natural chromaticities of (-14, -12).

With the phase advance per arc module set at $(\Delta\psi_x, \Delta\psi_y)|_{\rm module} = (8\pi/5, 6\pi/5,)$ contribution of the dipoles' average sextupole field to the $3\nu_x = 35$ resonance will cancel across one arc, but its contribution to the $\nu_x + 2\nu_y = 29$ resonance will build maximally across an arc, while cancelling across the ring. This cancellation depends on good adherence to superperidiocity, as will be discussed below.

3.3.4.3. Resonances

As suggested by Figure 3.3.3., it will be important to pick a good working point for the Proton Driver. We will discuss here the possible effects of two third integer resonances close to the working point of the base configuration, $\nu_x + 2\nu_y = 29$ and $3\nu_y = 26$, and (briefly) the $4\nu_y = 35$ resonance, which was seen in Figure 3.3.6. to be important in determining the dynamic aperture. In addition, see the discussion of phase advance in Section 3.4.

The effect of the $\nu_x - \nu_y = 3$ resonance on the tuned configuration was discussed in Section 3.3.4. A driver of the $2\nu_x - 2\nu_y = 6$ resonance will be space charge, a variant of the so-called "Montague resonance." Discussion of space charge effects is postponed to Chapter 4.

Most of the discussions in this section, and some in the preceding sections, are carried out using rough approximations. Applying isolated resonance theory validly requires satisfaction of many conditions. At the least, particle tunes must be very close to one and only one active resonant line, and no detuning must occur, apart from what is done by the resonance source itself. We will ignore the extent to which these conditions are violated.

$\underline{\nu_x + 2\nu_y = 29}$ The phase advance of $(\Delta\psi_x, \Delta\psi_y) = (8\pi/5, 6\pi/5)$ across an arc module means that the sextupoles' contribution to the $\nu_x + 2\nu_y = 29$ resonance driving term will add in phase from one module to the next. This is mitigated by the fact that 29 is an odd number, so that whatever resonance driving term is produced by one of the arcs should be cancelled by the other. Nonetheless, trusting in cancellations across opposite sides of a ring is risky. Superperiodicity of the lattice can be broken by the tuning quads in the straight sections, or simply because of field errors. A phase error between the two arcs will certainly arise. Estimating the effect of this resonance must take that into account.

A (moderately) "safe region" for the $\nu_x + 2\nu_y$ resonance is bounded by the curves [3, pp.233-238]

$$\begin{aligned}
\frac{1}{8}\left(\frac{\delta}{g}\right)^2 &= \frac{1}{4}\frac{\varepsilon_y}{\pi} + 2\left(\sqrt{\frac{\varepsilon_x}{2\pi}} - \frac{1}{4}\frac{|\delta|}{g}\right)^2 \quad , \\
\text{and} \quad -\frac{1}{4}\left(\frac{\delta}{g}\right)^2 &= 2\,\frac{\varepsilon_x}{\pi} - \frac{\varepsilon_y}{\pi} \quad , \\
\text{where} \quad g &= \frac{\sqrt{2}}{8\pi}\left|\sum \frac{B''l}{B\rho}\sqrt{\beta_x}\beta_y e^{i(\psi_x + 2\psi_y - \delta\cdot\theta)}\right| \quad ,
\end{aligned}$$

and $\delta = \nu_x + 2\nu_y - 29 = 0.12$. If sextupoles existed in all three of an arc module's cells, the value of g for one module would almost vanish, because $\langle \Delta(\psi_x + 2\psi_y)|_{\text{cell}} \rangle = (2/3)\cdot 2\pi$. However, for the base configuration as given, with sextupoles in two of the three cells, the value of g for one arc module is $\approx 1.36\ \text{m}^{-1/2}$. If we ignore the contribution from $\delta\cdot\theta$ in the exponent, then $g \approx 6.82\,\text{m}^{-1/2}$ across an arc, since $\Delta(\psi_x + 2\psi_y)|_{\text{module}} = 4\pi$. Let the

phase error between arcs be $\Phi \equiv \Delta\psi_x + 2\Delta\psi_y \pmod{2\pi}$. Then,

$$g_{\text{racetrack}} = 2\,|\sin(\Phi/2)|\,g_{\text{arc}} \quad .$$

The "safe regions" are plotted in Figure 3.3.8. for $\Phi \in \{45^\circ, 90^\circ, 135^\circ, 180^\circ\}$. Two squares

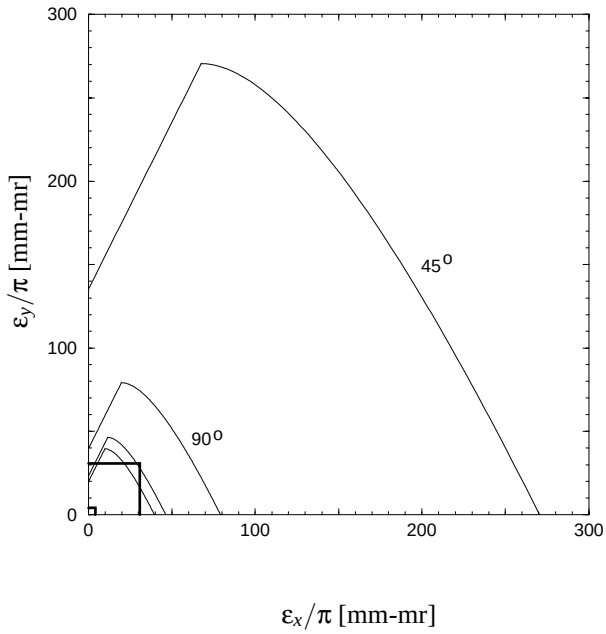

Figure 3.3.8. "Safe regions" for the $\nu_x + 2\nu_y$ resonance, in the base configuration, when $\Phi \in \{45^\circ, 90^\circ, 135^\circ, 180^\circ\}$, with invariant emittance of 40π mm-mr shown at injection and extraction. Ignoring space charge and second order sextupole effects, the injected beam is within the boundary provided $\Phi \ll 105^\circ$.

in the lower left corner show the beam emittances at injection and extraction. (See Eq.(3.1).) The boundary crosses the injected beam at $\Phi \approx 105^\circ$. Superperiodicity must be preserved to a value smaller than that.

This optimistic statement does not take into account the effects of space charge and (to second order) sextupoles in distributing tunes throughout the beam. How small, for example, must Φ be in order to reduce the "tune width" to $\delta \leq \pm 0.01$ for all particles at injection? Answering this is complicated by the fact that the largest tune shifts will occur near the core of the beam. For the sake of argument, let us say that 10% of the beam (emittance) gets shifted within reach of the resonance line. Then, we require that superperiodicity be preserved at the level $\Phi < 24^\circ$ or better, significantly more restrictive than the optical value of 105°. However, it is possible that space charge detuning could limit the instability produced by the resonance. [5] If the PD2 base configuration is seriously considered, this issue should be studied thoroughly. Near extraction, where particle tunes will be closer to the reference point, $\Phi < 21^\circ$ should be sufficient to allow moving the entire beam within ± 0.01 of the resonance line, although there is no reason to do so.

$3\nu_y = 26$ Even in the absence of field errors, the $3\nu_y = 26$ resonance can be excited in the base configuration by a roll misalignment of chromaticity sextupoles. The maximum vertical emittance contained within a (0,3) separatrix is,[3]

$$\begin{aligned} \varepsilon_{\max} &= \frac{2}{\sqrt{3}}\left(\frac{\delta}{g}\right)^2 , \text{ where} \\ \delta &\equiv 3\nu_y - 26 , \text{ and} \\ g &\equiv \frac{1}{12\sqrt{2}\,\pi}\left| \sum \left(\frac{B''_{\text{skew}} l}{B\rho}\right) \beta_y^{3/2} e^{i(3\psi_y - \delta\cdot\theta)} \right| . \end{aligned} \tag{3.2}$$

The sum is taken over all sources of skew sextupole: $\delta = 3\nu_y - 26$, assumed to be small, is the distance to the resonance line, g is the resonance coefficient, $\theta = s/R$ is the azimuthal coordinate around the ring, while β_y and ψ_y are vertical lattice functions at θ. When δ is sufficiently small, we can set $\delta = 0$ in the exponent of the integrand. If the field arises from a dipole error, then $B''_{\text{skew}} = 2Ba_2$, where B is the dipole field and a_2 is the skew sextupole coefficient; if it arises from rolling a normal sextupole through a small angle, Θ, then $B''_{\text{skew}} = B'' \cdot 3\Theta$. Thus, we can rewrite Eq.(3.2) as,

$$g = \frac{1}{12\sqrt{2}\,\pi}\left| \sum_{\text{dipoles}} 2a_2 \cdot \phi \cdot \beta_y^{3/2} e^{i(3\psi_y - \delta\cdot\theta)} + \sum_{\text{sextupoles}} \left(\frac{B''l}{B\rho}\right) \cdot (\,3\Theta\,) \cdot \beta_y^{3/2} e^{i(3\psi_y - \delta\cdot\theta)} \right| ,$$

where ϕ is the bend angle of a dipole. A systematic error is of little concern, because the phasors cancel remarkably well across an arc: $3\Delta\psi_y|_{\text{module}} = 18\pi/5 \simeq (-1/5)\cdot 2\pi$. To estimate the effect of random errors, we do the summation in quadrature.

$$\sigma_g^2 = \frac{1}{8\pi^2}\left[\frac{1}{9}\left(\sum_{\text{dipoles}} \phi^2 \beta_y^3\right)\sigma_{a_2}^2 + \frac{1}{4}\left(\sum_{\text{sextupoles}} \left(\frac{B''l}{B\rho}\right)^2 \beta_y^3\right)\sigma_\Theta^2\right]$$

We concern ourselves here only with the term arising from chromaticity sextupoles. For 20 of the 40 sextupoles, $B''l/B\rho \approx 0.50\,\text{m}^{-2}$ and $5.3\,\text{m} < \beta_y < 6.8\,\text{m}$, with a median value of 6.2 m; for the other 20, $B''l/B\rho \approx -0.72\,\text{m}^{-2}$ and $14.2\,\text{m} < \beta_y < 19.8\,\text{m}$, with a median value of 16.7 m. Thus we estimate,

$$\sigma_g^2\,[m^{-1}] = \frac{1}{32\pi^2}\cdot 20 \cdot \left(0.5^2 \cdot 6.2^3 + 0.72^2 \cdot 16.7^3\right) \cdot 0.0005^2 = 3.9 \times 10^{-5}$$

Putting this number into Eq.(3.2) we see that, at injection, maximum amplitude particles ($\varepsilon \approx 31\pi$ mm-mr) will feel the effect of this resonance when $\delta < 5.7 \times 10^{-5}$, a number too small to be considered threatening.

$4\nu_y = 35$ The tune diagram of Figure 3.3.6. suggests that the dynamic aperture is "seeded" [3, pp.281-284] upon the $4\nu_y = 35$ resonance. Since no octupoles were included in either the base or tuned configurations models, this line is excited by the sextupoles with a strength quadratic in $B''/B\rho$. The same sextupoles shift the tunes of large amplitude particles onto the line. (See page 3 - 9.) The importance of a $4\nu_y$ resonance and its effect on beam loss in ISIS has already been discussed in the PD1 Report. [1, p.3-18]

[3] One can choose from several rough approximations to develop this argument. The one used here employs the area of an equilateral triangle with vertices at the resonant orbits. To use the triangle's in-circle instead, replace "$2/\sqrt{3}$" with "$\pi/9$."

3.4. Alternative Designs

Several alternative lattice designs were considered, although not all were studied thoroughly. Some may eventually be revisited and new ones developed. For now we content ourselves with simply recording a few of them for future reference. One, the possibility of using combined function magnets, was already discussed in PD1. The three we consider here are: (a) changing the phase advance through the arc module, (b) eliminating the small dipole from the central cell of the arc module (MM: missing magnet), and (c) using a triangular, transitionless lattice (IG: imaginary γ_t). For convenient reference, a summary of their optical properties is provided below. Information on their hardware and space

Property (Lengths in meters)	PD2	MM (racetrack)	IG
$\Delta\psi_{\text{cell}}$	($8\pi/15$, $2\pi/5$)	($\pi/2$, $\pi/2$)	($\pi/2$,$\pi/2$)
Cells/arc	$3\times5=15$	$3\times4=12$	N/A
Cells/straight	7	6	4
(ν_x,ν_y)	(11.747, 8.684)	(9.048, 8.784)	(8.366,7.805)
max (β_x,β_y)	(15.141, 20.332)	(19.225, 20.695)	(41.363, 36.120)
min (β_x,β_y)	(4.105, 4.570)	(5.578, 4.642)	(1.014, 1.252)
max D_x	2.523	4.334	2.809
min D_x	0.0	-0.061	-3.819
α	0.0053	0.0066	-0.006
γ_t	13.758	12.349	N/A

Table 3.4.2. Optical properties of alternative lattices.

usage is compiled in Table 3.4.3., which should be compared with Table 3.2.1.. Lattice files, in MAD input format, for all of these can be found on the Proton Driver web site, http://www-bd.fnal.gov/pdriver/8GEV .

3.4.1. Alternative Phase Advance Lattices

The phase advance per arc module of the PD1 lattice, with four modules in an arc, was $(\Delta\psi_x,\Delta\psi_y)|_{\text{module}}=(3\pi/2,3\pi/2)$. When the number of modules was increased to five, the phase advance had to change to $(m_x\pi/5,m_y\pi/5)$, where m_x and m_y were integers. To zero the dispersion in the straight sections, (a) m_x should be even, and (b) each module should be a first order achromat. (If (b) is not satisfied, dispersion in the arcs won't be periodic across module boundaries.) The choice $m_x=8$ assures that γ_t is comfortably above the energy reach of the Proton Driver; $m_x=6$ results in insufficient horizontal focusing. For much of PD2 it was assumed that the average phase advance per cell was to be $(\Delta\psi_x,\Delta\psi_y)|_{\text{cell}}=(8\pi/15,\pi/3)=(96^\circ,60^\circ)$, corresponding to $m_x=8,m_y=5$, and making the vertical phase advance across a three-cell arc module, $\Delta\psi_y|_{\text{module}}=(1/2)\cdot2\pi$. However, when dipoles (with parallel edges) are introduced into the module, perturbations induced by the vertical edge focusing make it difficult to make the module a periodic, linearly stable unit in the vertical direction. It is sitting on top of the half-integer stop band.

Lattice	Element	Name	Number	Length [m]		Field	
MM	DIPOLES	B1	2x4x2 = 16	7.780	$B =$	1.49	T
	QUADRUPOLES	QF	(6+3x4)x2 = 36	1.059	$B' =$	10.29	T/m
		QD	(6+3x4)x2 = 36	1.059		-10.07	
	FREE (total)			273.401			
IG	DIPOLES	B2	3x2x3 = 18	7.88	$B =$	1.26	T
		B2145	2x2x3 = 12	2.95		1.26	T
	QUADRUPOLES	QFS+QFS	2x3 = 6	0.50	$B' =$	8.13	T/m
		QDS+QDS	1x3 = 3	0.50		-8.13	
		QDAF+QDS	2x3 = 6	0.50		-8.13	
		QDLBX	3x3 = 9	1.00		-8.13	
		QFLBX	3x2x3 = 18	1.00		8.13	
		QDLBY	2x2x3 = 12	0.72		-8.13	
		QFLBY	2x3 = 6	0.72		8.13	
		QDT	4x2x3 = 24	0.24		-2.03	
		QFT	2x3x3 = 18	0.24		2.03	
	SEXTUPOLES	HS1	2x3x3 = 18	0.25	$B'' =$	16.86	T/m^2
		VS1	2x3x3 = 18	0.25		-24.70	
		HS2	2x2x3 = 12	0.25		-16.86	
		VS2	2x2x3 = 12	0.25		24.70	
	FREE (total)			254.38			

Table 3.4.3. Hardware and space usage in two alternative designs: MM, the missing magnet lattice, and IG, the transitionless (imaginary γ_t) lattice.

Either the module is unstable vertically or its vertical lattice function, β_y, does not match well into the straight sections. Of course, *it is not necessary that the arc module be a linearly stable unit.* The arcs could act simply as beamlines connecting one straight section to the other. One design did, in fact, proceed in this manner, but not without using individually powered trim quads to control β_y in the arcs.

The choice was between (a) designs in which lattice functions in arcs and straight sections are automatically reasonably matched using the main bus quads, while trim quads are used for small perturbations, and (b) designs in which trim quads control lattice functions in the arcs, even in a "base" configuration. The phase advance was changed to $(\Delta\psi_x, \Delta\psi_y)|_{\text{module}} = (8\pi/5, 6\pi/5)$, corresponding to choice (a).[4] (As a bonus, the arcs were made optically transparent in both planes.) We have discussed the negative implications for the $\nu_x + 2\nu_y = 29$ resonance line when superperiodicity is broken. (See pp.3 - 16 *ff.*) If superperiodicity is preserved, tracking suggests that the most important resonance for determining dynamic aperture will be $4\nu_y = 35$, which could be excited by the $(8\pi/15, \pi/3)$ design as well. Finding a good working point will be an important operational consideration.

[4] A possibility that was not studied, but may be worth a look in the future, is $(\Delta\psi_x, \Delta\psi_y)|_{\text{module}} = (8\pi/5, 7\pi/5)$. The principle resonance of concern would then be $2\nu_x + 2\nu_y = 44$. Considering that there are 44 cells, and that the resonance can be driven by space charge, this numerology could be ominous.

3.4.2. Missing Magnet Lattice

In one variation of the PD2 design, the small dipoles are removed from the central cells of the arc modules. This increases the amount of free space in the arcs and eliminates about 40% of the momentum compaction (see page 3 - 8), raising transition gamma. Lengths and strengths of remaining elements are adjusted so that the arc module remains a linear achromat. The "missing magnet" design had the attractiveness of featuring only a single species of quadrupole and dipole, making it one of the simplest lattices considered. It was not pursued because its maximum dispersion of ≈ 3 m, with $\beta_{x,\max} \approx 26$ m and $\beta_{y,\max} \approx 30$ m, were too large to accomodate $\varepsilon_{\text{inv}} = 40\pi$ mm-mr at injection.

3.4.3. Transitionless Lattice

One of the superperiod 3, triangular lattices considered is noteworthy in that it possesses a negative momentum compaction, α. It is a so-called "imaginary γ_t" lattice, which more correctly means that it is transitionless: there is no energy for which the slip factor, $\alpha - 1/\gamma^2$, becomes positive. Each arc contains three low β_x regions and two low β_y regions. Low β_y regions coincide with regions of negative dispersion, which make α negative. Unfortunately, small β in one location generally requires large β elsewhere. Like the missing magnet design, this one was not pursued because its maximum dispersion (magnitude) of ≈ 3.8 m was too large when combined with $\beta_{x,\max} \approx 41$ m and $\beta_{y,\max} \approx 36$ m.

3.4.4. References

[1] R. Alber, *et al.*, The proton driver design study. Technical report, Fermilab, December, 2000. Fermilab-TM-2136.

[2] A. Piwinski. Handbook of Accelerator Physics and Engineering, p.72. Edited by A. Chao and M. Tigner.

[3] L. Michelotti. *Intermediate Classical Dynamics with Applications to Beam Physics*. John Wiley & Sons, Inc., New York, 1995.

[4] D. A. Edwards and M. J. Syphers. *An Introduction to the Physics of High Energy Accelerators*. John Wiley & Sons, New York, 1993.

[5] I. Hofmann, A. Fedotov, and G. Franchetti. Space charge resonances in high intensity drivers. Presented at 20th ICFA Advanced Beam Dynamics Workshop: High Intensity High Brightness Hadron Beams. Fermilab., April 8-12 2002.